SAR COMPLIANCE TESTING OF ALCATEL

MODEL 4073 GS TELEPHONE

FINAL TECHNICAL REPORT

May 17, 1999

Submitted to:

Mr. Joe Jackson
VP, Marketing
Communication Certification Laboratory
1940 West Alexander Street
Salt Lake City, UT 84119-2039

Submitted by:

Om P. Gandhi
Professor and Chairman
University of Utah
Electrical Engineering Department
50 S Central Campus Dr., Rm. 3280
Salt Lake City, UT 84112-9206

SAR COMPLIANCE TESTING OF ALCATEL
MODEL 4073 GS TELEPHONE

I. Introduction

The U.S. Federal Communications Commission (FCC) has adopted limits of human exposure to RF emissions from mobile and portable devices that are regulated by the FCC [1]. The FCC has also recently issued Supplement C (Edition 97-01) to OET Bulletin 65 defining both the measurement and the computational procedures that should be followed for evaluating compliance of mobile and portable devices with FCC limits for human exposure to radiofrequency emissions [2].

For Alcatel Model 4073 GS Telephone, we have used the experimental measurement techniques to determine the SAR distributions from which the peak 1-g SARs are obtained, as recommended in [2]. This telephone (see Fig. 1) has a built-in inverted L-antenna of approximate dimensions 2.0-2.2 cm for each of the two legs. As recommended in [2], the telephone is placed against the left ear of the human-shaped model which is filled with a brain-simulant fluid. Also as recommended in [2], the handset is tested without the model of a hand to determine once again the worst case SAR distribution (see Fig. 2).

II. The Alcatel Model 4073 GS Telephone

The Alcatel Model 4073 GS Telephone operates in one of eight channels 0-7 with frequencies as follows:

Channel	Frequency MHz
0	1929.375
1	1928.125
2	1926.875
3	1925.625
4	1924.375
5	1923.125
6	1921.875
7	1920.625

The rated peak power output of the device is approximately 17 dBm (50 mW) with a duty cycle of 1/24 i.e. a source-based time-averaged conducted power of approximately 2.1 mW. We were, however, provided with a second telephone where the antenna was removed and the output of the power amplifier brought out by means of an RG 178 coaxial cable of length 12 cm. Using this second identical telephone, we measured the power output of the power amplifier of the telephone. The power measured for each of the transmit channels using the Hewlett Packard (HP) Model 436A Power Meter with HP Model 8481H Power Sensor is given in Table 1. Since the attenuation of the RG 178 coaxial cable, including the connectors, is on the order of 1 dB, the corrected output powers for each of the channels are also given in Table 1.

III. The Tissue-Simulant Model

For measurements of SAR distributions, we have used the Utah Experimental Model that is described in detail in [4]. This model uses a lossy outer shell of the following approximate dimensions:

Axial length from chin to top of the head = 26 cm
Distance from location of the ear canal to top of the head = 14.7 cm
Width from side to side = 16.5 cm

These dimensions are typical for adult human beings. The shell thickness of the head and neck model is approximately 4-7 mm, which is typical of the human skull thickness. The thickness for the ear region is, however, considerably less and is only about 3 mm.

This experimental model shown in Fig. 2 has, in the past, been used for comparison of the measured peak 1-g SARs with those obtained with the Utah FDTD Code for ten wireless telephones, five at 835 MHz and five for PCS (1900 MHz) frequencies [see Table 2]. The numerical SARs were obtained using the anatomically-based, 15-tissue Utah model of the head and neck with a resolution of $1.974 \times 1.974 \times 3.0$ mm that has been described in the scientific literature through numerous publications (see e.g. references 3, 5). The measured and calculated 1-g SARs for these ten telephones,

including some research test samples from diverse manufacturers using a variety of radiating antennas for different source-based time-averaged powers are compared in Table 2 [4]. Even though widely different peak 1-g SARs from 0.13 to 5.41 W/kg are obtained because of the variety of antennas and handsets, agreement between the calculated and the measured data is excellent and generally within ± 25 percent.

These tests validate the Utah Experimental Phantom Model as being capable of giving peak 1-g SARs that are in good agreement with the SARs obtained with the realistic, anatomically-based model of the human head and neck both at 835 and 1900 MHz.

The head and neck and the upper part of the torso of the model are filled with a liquid with measured electrical properties (dielectric constant and conductivity) close to the average properties of the brain for white and gray matters at 1925 MHz which is close to the midband transmission frequency for this telephone. This composition [4] developed in our laboratory consists of 60% water, 18.0% sugar, 20% polyethylene powder (PEP), 0.4% NaCℓ and 1.6% protein-based gelling agent TX151 (available from Oil Center Research Inc., LaFayette, LA). As measured in our laboratory using the HP Model 85070B Dielectric Probe in conjunction with HP Model 8720C Network Analyzer (50 MHz-20 GHz), this composition gives a measured $\varepsilon_r = 45.5 \pm 1.7$ and $\sigma = 1.31 \pm 0.06$ S/m. From reference 6, we obtained the desired dielectric properties to simulate the brain tissue at 1925 MHz to be $\varepsilon_r = 43.2$ and $\sigma = 1.29$ S/m. Thus the measured properties for the brain-simulant fluid used for experimental SAR measurements are close to the desired values.

IV. The E-Field Probe

The non-perturbing implantable E-field probe used in the setup was originally developed by Bassen et al. [7] and is now manufactured by L3/Narda Microwave Corporation, Hauppauge, New York as Model 8021 E-field probe. In this probe, three orthogonal miniature dipoles are placed on a triangular beam substrate. Each dipole is

loaded with a small Schottky diode and connected to the external circuitry by high resistance (2 MΩ ± 40%) leads to reduce secondary pickups. The entire structure is then encapsulated with a low dielectric constant insulating material. The probe thus constructed has a very small (4 mm) diameter, which results in a relatively small perturbation of the internal electric field.

Test for Square Law Region

It is necessary to operate the E-field probe in the square law region for each of the diodes so that the sum of the dc voltage outputs from the three dipoles is proportional to the square of the internal electric field ($|E_i|^2$). Fortunately, the personal wireless devices induce SARs that are generally less than 5-6 W/kg even for closest locations of the head [3]. For compliance testing, it is, therefore, necessary that the E-field probe be checked for square law behavior for SARs up to such values that are likely to be encountered. Such a test may be conducted using a canonical lossy body such as a rectangular box or a sphere irradiated by a dipole. By varying the radiated power of the dipole, the output of the probe should increase linearly with the applied power for each of the test locations.

Shown in Figs. 3a, 3b are the results of the tests performed to check the square law behavior of the E-field probe used in our setup at 840 and 1900 MHz, respectively. For these measurements, we have used a rectangular box of dimensions 30 × 15 × 50 cm that was irradiated by the corresponding half wave dipoles with different amounts of radiated powers from 200-800 mW. Since the dc voltage outputs of the probe are fairly similar when normalized to a radiated power of 100 mW, the square law behavior is demonstrated and an output voltage that is proportional to $|E_i|^2$ is obtained within ± 3 percent.

Test for Isotropy of the Probe

Another important characteristic of the probe that affects the measurement accuracy is its isotropy. Since the orientation of the induced electric field is generally unknown, the E-field probe should be relatively isotropic in its response to the orientation of the E-field. Shown in Figs. 4a, 4b are the test results of the E-field probe used in our setup at 840 and

1900 MHz, respectively. The previously described box phantom of dimensions 30 × 15 × 50 cm along x, y and z dimensions, respectively, was also used for these measurements. This phantom was filled to a depth of 15 cm with brain-simulant materials (Table 3). The E-field probe was rotated around its axis from 0 to 360° in incremental steps of 60°. An isotropy of less than ± 0.23 dB (± 5.5%) was observed for this E-field probe both at 840 and 1900 MHz.

Calibration of the E-Field Probe

Since the voltage output of the E-field probe is proportional to the square of the internal electric field ($|E_i|^2$), the SAR, given by $\sigma|E_i|^2/\rho$ is, therefore, proportional to the voltage output of the E-field probe by a proportionality constant C. The constant C is defined as the calibration factor, and is frequency and material dependent. It is measured to calibrate the probe at the various frequencies of interest using the appropriate tissue-simulating materials for the respective frequencies.

Canonical geometries such as waveguides, rectangular slabs and layered or homogeneous spheres have, in the past, been used for the calibration of the implantable E-field probe [8-10]. Since the Finite Difference Time Domain (FDTD) has been carefully validated to solve electromagnetic problems for a variety of geometries [11, 12], we were able to calibrate the Narda E-field probe by comparing the measured variations of the probe voltage ($\approx |E_i|^2$) against the FDTD-calculated variations of SARs for a box phantom of dimensions 30 × 15 × 50 cm used previously for the data given in Figs. 3 and 4, respectively. For these measurements, we placed the nominal half-wave dipoles of lengths 178 mm and 77 mm at 840 and 1900 MHz, respectively, at several distances d (see inserts of Figs. 5a, 5b, and 6a, 6b) from the outer surface of the acrylic (ε_r = 2.56) box of thickness 6.55 mm. Shown in Figs. 5a, 5b and 6a, 6b are the comparisons between the experimentally measured and FDTD-calculated variations of the SAR distributions for this box phantom. Since there are excellent agreements between the calculated SARs and the measured variations of the voltage output of the E-field probe for four different separations

d of the half wave dipoles at each of the two frequencies, it is possible to calculate the calibration factors at the respective frequencies. For the Narda Model 8021 E-field probe used in our setup, the calibration factors are determined to be 0.49 and 0.84 (mW/kg)/μV at 840 and 1900 MHz, respectively..

V. Experimental Results: Canonical Problems

To further validate the system, it has been used to measure the peak 1-g SAR for the above-mentioned box phantom and a glass sphere model of thickness 5 mm, external diameter = 223 mm and assumed dielectric constant $\varepsilon_r = 4.0$. This sphere model is once again filled with the corresponding brain-simulant fluids of compositions given in Table 3. Shown in Figs. 7a, 7b and 8a, 8b are the measured and FDTD-calculated SAR distributions inside the sphere for various separations d between the dipole and the sphere (see insert for Figs. 7, 8). Comparison of the measured and FDTD-calculated peak 1-g SARs for both phantom geometries are given in Tables 4 and 5, respectively. As can be seen, the agreement between experimental measurement and numerical simulation is excellent and generally within ± 10 percent for both rectangular and spherical phantoms.

VI. Measurement Uncertainty: Test Runs With Cellular Telephones

The automated setup shown in Fig. 3 of [4] has been used for the testing of ten personal wireless devices including some research test samples, five each at 835 and 1900 MHz, respectively. Given in Table 2 is the comparison of the numerical and measured peak 1-g SARs for these devices using our experimental phantom model and the FDTD-based numerical procedure used for calculations of SAR distributions for an anatomically-based model of the head of an adult male [4]. The measured and calculated SARs for the ten telephones which have quite different operational modes (TDMA, CDMA, etc.) and antenna structures (helical, monopole, or helix-monopole) vary from 0.13 to 5.41 W/kg. Even though widely different peak 1-g SARs are obtained because of the variety of

antennas and handsets, agreement between the calculated and the measured data is excellent and generally within ± 25%. This is particularly remarkable since an MRI-derived, 16-tissue anatomically-based model of the adult human head is used for FDTD calculations and a relatively simplistic two tissue phantom model is used for experimental peak 1-g SAR measurements.

We estimate the uncertainty of our measuring system to be ± 12.5 percent. As seen in Table 2, an agreement within ± 25 percent is obtained for the peak 1-g SARs calculated using the Utah FDTD Code and the Utah Experimental Phantom Model for ten assorted wireless devices using a variety of antennas and handset dimensions. Since both the numerical and experimental methods are completely independent methods, and each is prone to its own set of errors, an uncertainty of ± 12.5 percent can be ascribed to each of the methods.

VII. The Measured SAR Distributions for Alcatel Model 4073 GS Telephone

As suggested in Supplement C (Edition 97-01) to the FCC OET Bulletin 65 [2], the SAR measurements have been conducted with the Alcatel Model 4073 Telephone pressed against the model of the head such that the center of the ear piece is aligned against the location of the ear canal. Furthermore, the handset is oriented such that the center line of the body of the handset is in the plane passing through the two ear canals and the tip of the mouth.

Due to the very low conducted power on the order of 1.4 mW (see Table 1), the SARs are very low. It was, therefore, decided to search with a coarse scan with a step size of 8 mm three overlapping regions each of dimensions 4.8 × 7.2 cm to cover a total region with overall dimensions of 4.8 × 14.4 cm i.e. all of the region of the phantom model close to the Alcatel Model 4073 GS Telephone. In order to be certain that the low SARs that we were observing were indeed due to the Alcatel telephone, the microwave power radiated by the telephone was shut off and the background noise measured for each of the three

coarsely scanned regions called Areas 1, 2, and 3. The data on the background noise thus measured is given in Table 6 and can be seen to be very low indeed.

Having determined that the background readings were much smaller than the SARs caused by RF radiation from the Alcatel Model 4073 GS telephone, we proceeded to obtain the peak 1-g SARs for each of the three areas by first identifying the region of the highest SAR by a coarse scan with a step size of 8 mm and then covering the "hot spot" thus identified with a finer resolution of 2.0 mm. For all of these measurements, we decided to use channel 3 with a frequency of 1925.625 MHz which is close to the center band for this telephone. The detailed SAR distributions measured for the $1 \times 1 \times 1$ cm highest SAR region for each of the three scanned areas (1, 2, and 3) are given in Tables 7, 8, and 9, respectively. The peak 1-g SARs for these regions are 0.019, 0.015, and 0.013 W/kg. All of these SARs are almost two orders lower than the peak 1-g SAR of 1.6 W/kg suggested in the FCC 96-326 Guidelines [1].

VIII. Comparison of the Data With FCC 96-326 Guidelines

According to the FCC 96-326 Guidelines [1], the peak SAR for any 1-g of tissue should not exceed 1.6 W/kg. We have determined the peak 1-g SAR for the Alcatel Model 4073 GS Telephone to be 0.019 W/kg. This is considerably lower than 1.6 W/kg suggested in the FCC 96-326 Guidelines [1].

REFERENCES

1. Federal Communications Commission, "Guidelines for Evaluating the Environmental Effects of Radiofrequency Radiation," FCC 96-326, August 1, 1996.

2. K. Chan, R. F. Cleveland, Jr., and D. L. Means, "Evaluating Compliance With FCC Guidelines for Human Exposure to Radiofrequency Electromagnetic Fields," Supplement C (Edition 97-01) to OET Bulletin 65, December, 1997. Available from Office of Engineering and Technology, Federal Communications Commission, Washington D.C., 20554.

3. O. P. Gandhi, G. Lazzi and C. M. Furse, "Electromagnetic Absorption in the Human Head and Neck for Mobile Telephones at 835 and 1900 MHz," *IEEE Transactions on Microwave Theory and Techniques*, Vol. 44, pp. 1884-1897, 1996.

4. Q. Yu, O. P. Gandhi, M. Aronsson, and D. Wu, "An Automated SAR Measurement System for Compliance Testing of Personal Wireless Devices," accepted for publication in *IEEE Transactions on Electromagnetic Compatibility.*

5. O. P. Gandhi, "FDTD in Bioelectromagnetics: Safety Assessment and Medical Applications," Chapter 11, pp. 613-651 in *Advances in Computational Electrodynamics: The FDTD Method*, edited by A. Taflove, Artech House Inc., Dedham, MA, 1998.

6. C. Gabriel, Compilation of the Dielectric Properties of Body Tissues at RF and Microwave Frequencies," Technical Report AL/OE-TR-1996-0037, Armstrong Laboratory, Air Force Materiel Command, Brooks Air Force Base, Texas 78235, June 1996.

7. H. I. Bassen and G. S. Smith, "Electric Field Probes -- A Review," *IEEE Trans. Antennas Propagation*, Vol. 34, pp. 710-718, September 1983.

8. D. Hill, "Waveguide Techniques for the Calibration of Miniature Electric Field Probes for Use in Microwave Bioeffects Studies," *IEEE Trans. Microwave Theory Tech.*, Vol. 30, pp. 92-94, 1982.

9. N. Kuster and Q. Balzano, "Energy Absorption Mechanism by Biological Bodies in the Near Field of Dipole Antennas Above 300 MHz," *IEEE Trans. Veh. Technology,* Vol. 41, pp. 17-23, 1992.

10. M. A. Stuchly, S. S. Stuchly, and A. Kraszewski, "Implantable Electric Field Probes -- Some Performance Characteristics," *IEEE Trans. Biomed. Eng.*, Vol. 31, pp. 526-531, 1984.

11. A. Taflove, K. R. Umashankar, T. G. Jurgens, "Validation of FDTD Modeling of the Radar Cross Section of Three-Dimensional Structures Spanning Up to Nine Wavelengths," *IEEE Trans. Antennas and Propagation*, pp. 662-666, 1985.

12. C. M. Furse, Q. Yu, and O. P. Gandhi, "Validation of the Finite-Difference Time-Domain Method for Near-Field Bioelectromagnetic Simulations," *Microwave and Optical Technology Letters*, Vol. 16, pp. 341-345, 1997.

Table 1. The time-averaged conducted power of the Alcatel Model 4073 GS Telephone.

Channel #	Frequency MHz	Measured Power Output mW	Loss-Corrected* Power Output mW
0	1929.375	1.105	1.391
1	1928.125	1.105	1.391
2	1926.875	1.100	1.385
3	1925.625	1.103	1.389
4	1924.375	1.095	1.379
5	1923.125	1.103	1.389
6	1921.875	1.098	1.382
7	1920.625	1.090	1.372

* Because of 1 dB loss in the output coaxial cable and the connectors, the actual power output is higher than the measured output power.

Table 2. Comparison of the experimentally measured and FDTD-calculated peak 1-g SARs for ten wireless telephones, five each at 835 and 1900 MHz, respectively.

	Time-Averaged Radiated Power mW	Using Experimental Model W/kg	Numerical Method W/kg
Cellular Telephones at 835 MHz			
Telephone A	600	4.02	3.90
Telephone B	600	5.41	4.55
Telephone C	600	4.48	3.52
Telephone D	600	3.21	2.80
Telephone E	600	0.54	0.53
PCS Telephones at 1900 MHz			
Telephone A	125	1.48	1.47
Telephone B	125	0.13	0.15
Telephone C	125	0.65	0.81
Telephone D	125	1.32	1.56
Telephone E	99.3	1.41	1.25

Table 3. Compositions used for brain-equivalent materials.

840 MHz		1900 MHz	
Water	40.4%	Water	60.0%
Sugar	56.0%	Sugar	18.0%
Salt (NaCl)	2.5%	PEP	20.0%
HEC	1.0%	Salt (NaCl)	0.4%
		TX 151	1.6%
$\varepsilon_r = 41.1 \pm 1.4$		$\varepsilon_r = 45.5 \pm 1.7$	
$\sigma = 1.06 \pm 0.05$ S/m		$\sigma = 1.31 \pm 0.06$ S/m	

Table 4. Box phantom: Comparison of the measured and FDTD-calculated peak 1-g SARs for four spacings each at 840 and 1900 MHz, radiated power normalized to 0.5 W.

Frequency (MHz)	Distance (mm) Between λ/2 Dipole and the Box	SAR (W/kg)		Difference (%)
		Measured	FDTD	
840	17.5	4.58	4.20	+8.3
840	22.5	3.53	3.65	-3.4
840	27.5	2.69	3.00	-10.2
840	33.0	1.95	2.24	-12.9
1900	16.5	7.45	7.46	-0.1
1900	21.5	4.24	4.18	+1.4
1900	26.5	2.71	2.91	-7.9
1900	31.5	1.77	1.75	+1.1

Table 5. Sphere phantom: Comparison of the measured and FDTD-calculated peak 1-g SARs for three spacings each at 840 and 1900 MHz, radiated power normalized to 0.5 W.

Frequency (MHz)	Distance (mm) Between λ/2 Dipole and the Box	SAR (W/kg)		Difference (%)
		Measured	FDTD	
840	5	6.78	6.77	+0.23
840	15	3.41	3.27	+4.22
840	25	1.85	1.68	+9.51
1900	5	17.45	18.01	-3.21
1900	15	4.96	5.05	-1.81
1900	25	1.69	1.77	-4.73

Table 6. The background noise measurements (in units of W/kg) for three coarse scan areas each of dimensions 4.8 × 7.2 cm measured with a resolution of 8 mm.

Area 1

0.001	0.000	0.000	0.001	0.001	0.001	0.001
0.001	0.002	0.002	0.001	0.001	0.001	0.002
0.001	0.003	0.001	0.001	0.002	0.002	0.001
0.002	0.002	0.003	0.001	0.002	0.003	0.002
0.003	0.002	0.003	0.002	0.002	0.001	0.003
0.003	0.002	0.002	0.003	0.001	0.003	0.002
0.003	0.002	0.002	0.002	0.002	0.002	0.003
0.001	0.001	0.003	0.003	0.002	0.003	0.002
0.002	0.002	0.002	0.002	0.001	0.002	0.002
0.003	0.003	0.002	0.001	0.002	0.002	0.003

Area 2

0.003	0.000	0.001	0.000	0.001	0.001	0.001
0.002	0.002	0.001	0.002	0.001	0.001	0.000
0.003	0.002	0.001	0.002	0.002	0.002	0.002
0.003	0.002	0.002	0.002	0.002	0.001	0.001
0.002	0.003	0.002	0.002	0.002	0.002	0.001
0.003	0.003	0.001	0.002	0.001	0.002	0.003
0.002	0.003	0.002	0.001	0.002	0.004	0.002
0.001	0.002	0.003	0.001	0.002	0.004	0.002
0.002	0.001	0.002	0.002	0.002	0.003	0.002
0.001	0.002	0.001	0.002	0.002	0.002	0.001

Area 3

0.003	0.000	0.003	0.001	0.002	0.002	0.002
0.002	0.003	0.001	0.002	0.003	0.002	0.002
0.000	0.001	0.002	0.002	0.002	0.003	0.002
0.002	0.002	0.002	0.002	0.002	0.001	0.001
0.002	0.002	0.002	0.002	0.002	0.002	0.003
0.002	0.002	0.001	0.002	0.001	0.001	0.001
0.002	0.002	0.003	0.002	0.003	0.002	0.003
0.002	0.003	0.002	0.002	0.001	0.003	0.002
0.003	0.003	0.003	0.003	0.002	0.002	0.002
0.001	0.002	0.002	0.001	0.001	0.002	0.002

Table 7. **Alcatel Model 4073 GS Telephone.** The SAR distribution (in W/kg) measured with a resolution of 2 mm for the highest SAR region for scanned area 1 (covering the top 5 cm of the telephone and an additional height of 2.2 cm above it).

Peak 1-g SAR = 0.019 W/kg

a. At depth of 1 mm

0.025	0.020	0.026	0.023	0.025
0.025	0.024	0.025	0.028	0.028
0.031	0.027	0.027	0.024	0.028
0.030	0.025	0.026	0.023	0.025
0.024	0.025	0.026	0.025	0.028

b. At depth of 3 mm

0.022	0.019	0.021	0.020	0.020
0.022	0.021	0.021	0.022	0.022
0.024	0.022	0.022	0.021	0.022
0.024	0.022	0.022	0.020	0.021
0.021	0.022	0.021	0.021	0.022

c. At depth of 5 mm

0.019	0.017	0.017	0.017	0.017
0.019	0.018	0.017	0.018	0.017
0.019	0.018	0.018	0.018	0.017
0.019	0.019	0.018	0.018	0.017
0.018	0.019	0.017	0.017	0.017

d. At depth of 7 mm

0.016	0.016	0.014	0.014	0.014
0.016	0.015	0.015	0.015	0.014
0.015	0.015	0.015	0.016	0.014
0.015	0.016	0.016	0.016	0.015
0.015	0.016	0.014	0.015	0.014

e. At depth of 9 mm

0.014	0.014	0.012	0.013	0.012
0.014	0.013	0.013	0.013	0.013
0.013	0.013	0.013	0.014	0.012
0.013	0.014	0.014	0.014	0.013
0.013	0.014	0.012	0.013	0.013

Table 8. **Alcatel Model 4073 GS Telephone.** The SAR distribution (in W/kg) measured with a resolution of 2 mm for the highest SAR region for scanned area 2 covering the central part of the telephone.

Peak 1-g SAR = 0.015 W/kg

a. At depth of 1 mm

0.020	0.020	0.022	0.024	0.023
0.020	0.024	0.020	0.024	0.026
0.024	0.023	0.024	0.019	0.022
0.022	0.021	0.024	0.021	0.019
0.021	0.020	0.019	0.024	0.026

b. At depth of 3 mm

0.017	0.017	0.017	0.018	0.018
0.017	0.019	0.017	0.018	0.019
0.018	0.018	0.019	0.016	0.017
0.019	0.018	0.019	0.018	0.016
0.018	0.017	0.016	0.019	0.019

c. At depth of 5 mm

0.015	0.013	0.013	0.014	0.014
0.015	0.015	0.014	0.014	0.014
0.014	0.014	0.015	0.014	0.013
0.016	0.015	0.015	0.015	0.013
0.015	0.015	0.014	0.014	0.014

d. At depth of 7 mm

0.013	0.011	0.010	0.011	0.012
0.012	0.012	0.011	0.011	0.011
0.011	0.011	0.012	0.012	0.011
0.013	0.012	0.012	0.012	0.011
0.012	0.013	0.012	0.011	0.011

e. At depth of 9 mm

0.011	0.009	0.008	0.009	0.010
0.010	0.010	0.009	0.009	0.009
0.009	0.009	0.010	0.010	0.009
0.011	0.010	0.010	0.010	0.010
0.010	0.011	0.010	0.009	0.010

Table 9. **Alcatel Model 4073 GS Telephone.** The SAR distribution (in W/kg) measured with a resolution of 2 mm for the highest SAR region for scanned area 3 covering the lower part of the telephone.

Peak 1-g SAR = 0.013 W/kg

a. At depth of 1 mm

0.017	0.021	0.019	0.019	0.022
0.019	0.017	0.019	0.018	0.021
0.018	0.015	0.019	0.018	0.018
0.013	0.015	0.015	0.012	0.018
0.015	0.013	0.014	0.013	0.017

b. At depth of 3 mm

0.016	0.018	0.016	0.016	0.017
0.016	0.016	0.016	0.015	0.016
0.015	0.013	0.015	0.015	0.014
0.012	0.013	0.013	0.012	0.014
0.013	0.012	0.012	0.012	0.013

c. At depth of 5 mm

0.015	0.015	0.014	0.014	0.014
0.014	0.015	0.014	0.013	0.013
0.013	0.011	0.013	0.013	0.012
0.012	0.011	0.011	0.012	0.012
0.011	0.011	0.010	0.011	0.009

d. At depth of 7 mm

0.013	0.013	0.012	0.012	0.012
0.013	0.013	0.012	0.012	0.011
0.011	0.010	0.011	0.011	0.010
0.011	0.010	0.010	0.011	0.011
0.010	0.010	0.009	0.010	0.008

e. At depth of 9 mm

0.012	0.011	0.011	0.011	0.011
0.011	0.012	0.011	0.010	0.010
0.010	0.010	0.010	0.010	0.010
0.010	0.010	0.010	0.010	0.010
0.010	0.009	0.009	0.009	0.008

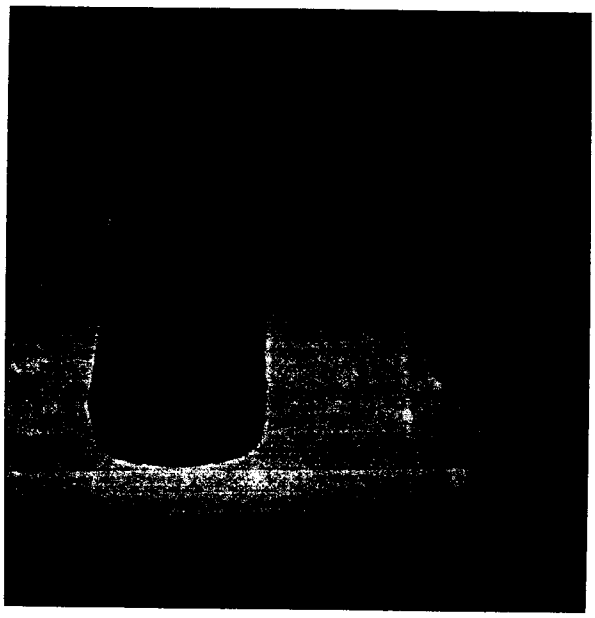

Fig. 1. Photograph of the Alcatel Model 4073 GS Telephone. Note the lack of a protruding antenna since this telephone uses an inverted-L built-in antenna.

Fig. 2. The phantom model used for measurement of the SAR distribution for Alcatel Model 4073 GS Telephone.

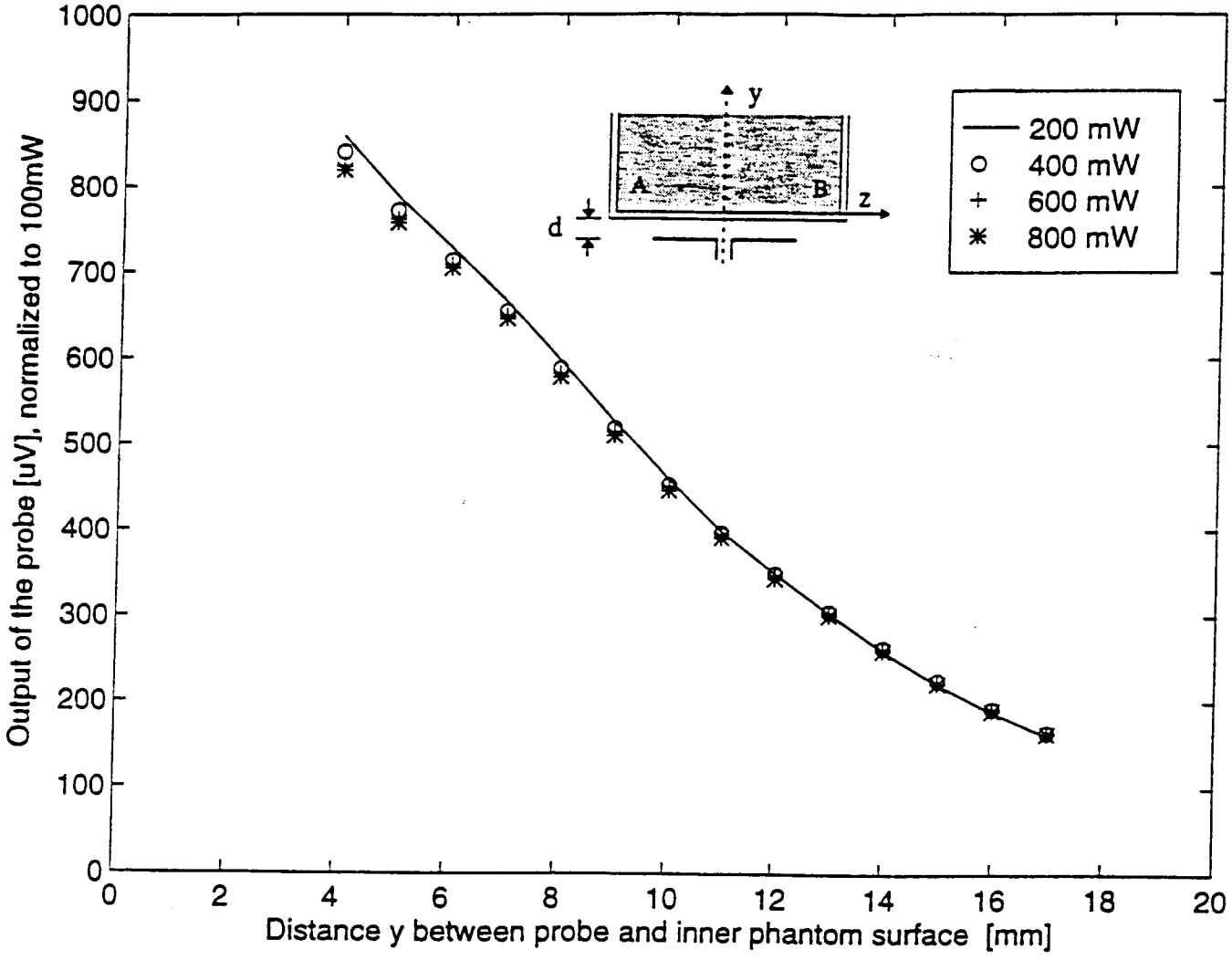

Fig. 3. Test for square-law behavior at 1900 MHz: Variation of the output voltage (proportional to $|E_i|^{2)}$ for different radiated powers normalized to 0.1 W.

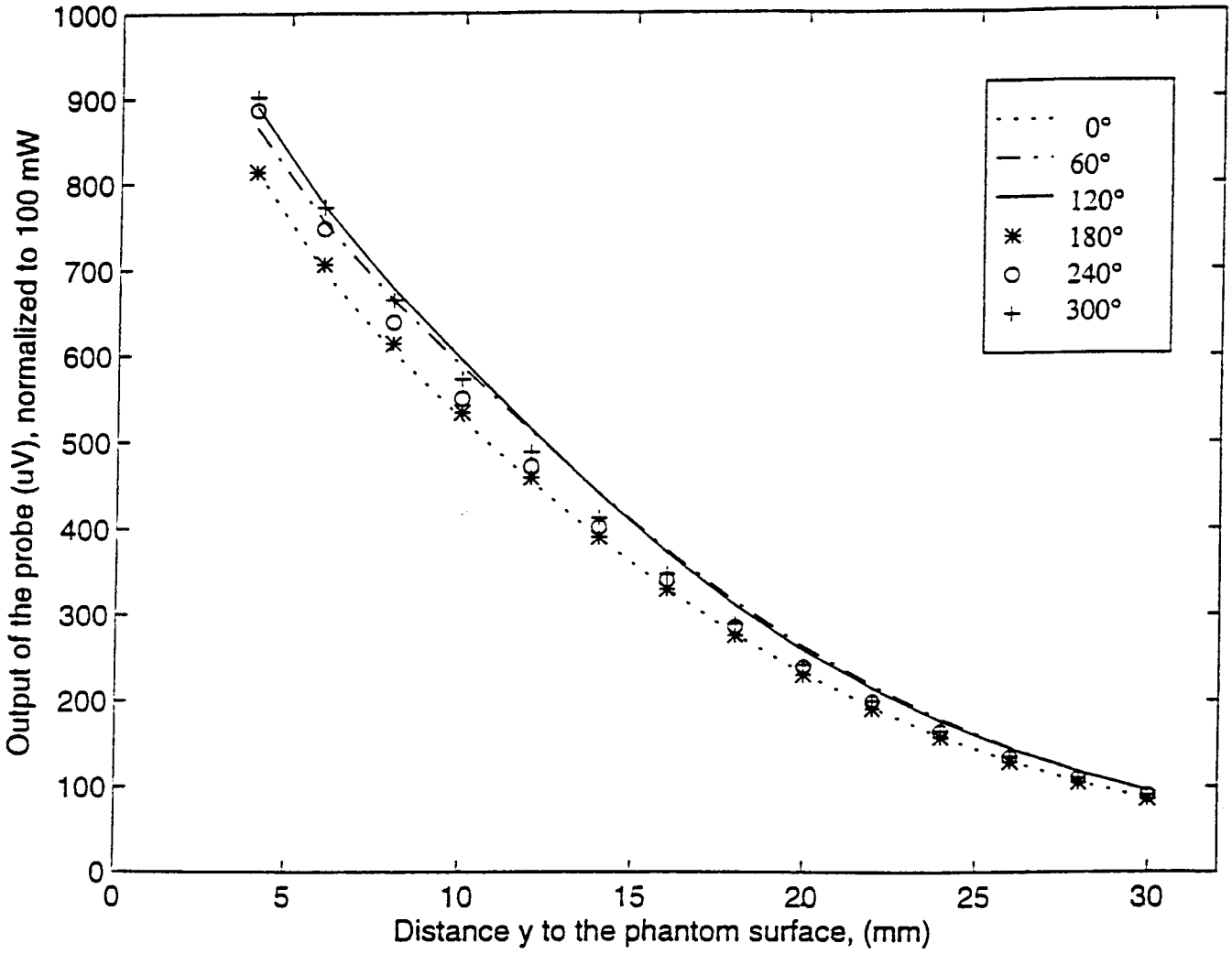

Fig. 4a. Test for isotropy: The model shown in Fig. 1 was used with nominal half wavelength dipole radiator of length 178 mm at 840 MHz.

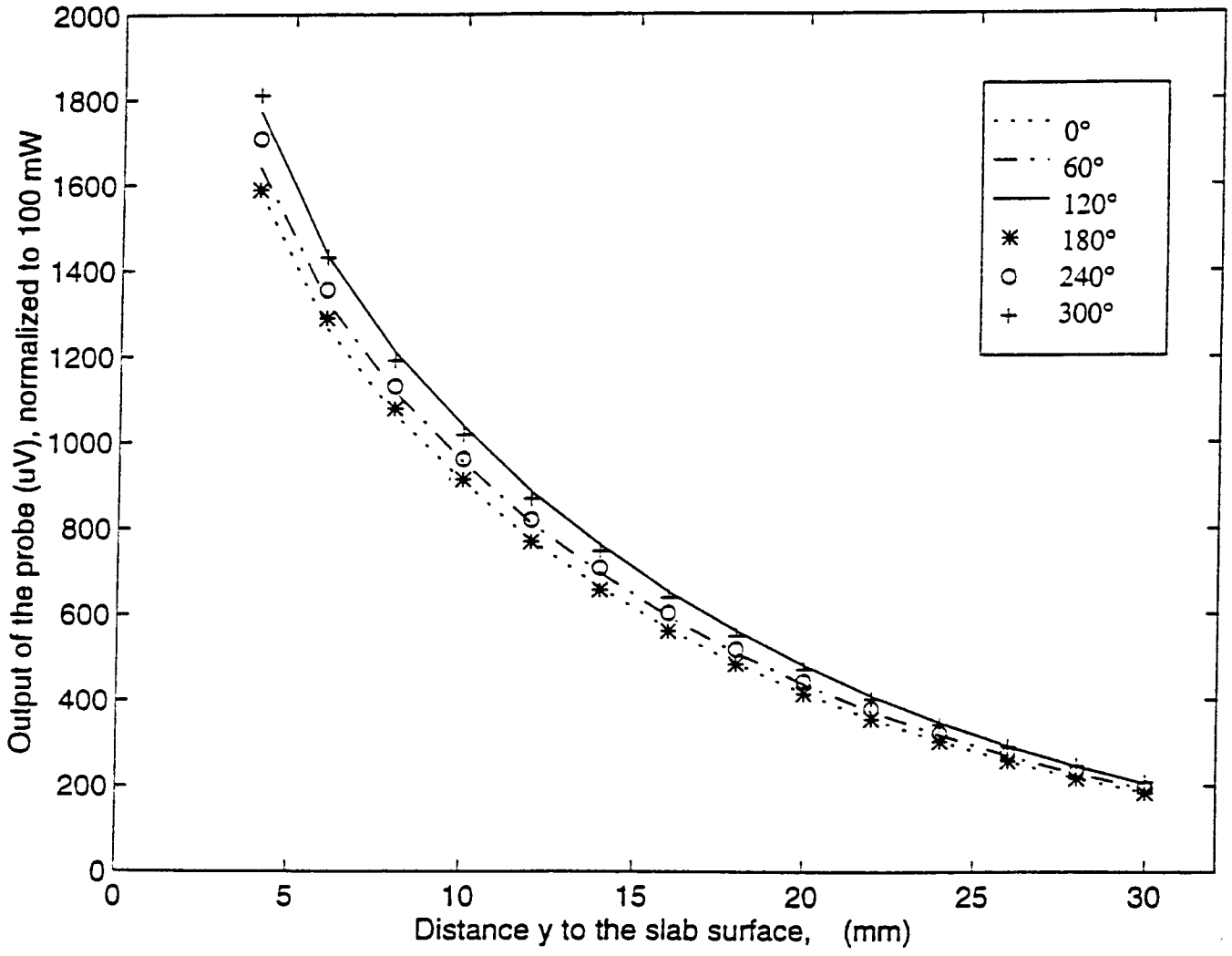

Fig. 4b. Test for isotropy: The model shown in Fig. 1 was used with nominal half wavelength dipole radiator of length 77 mm at 1900 MHz.

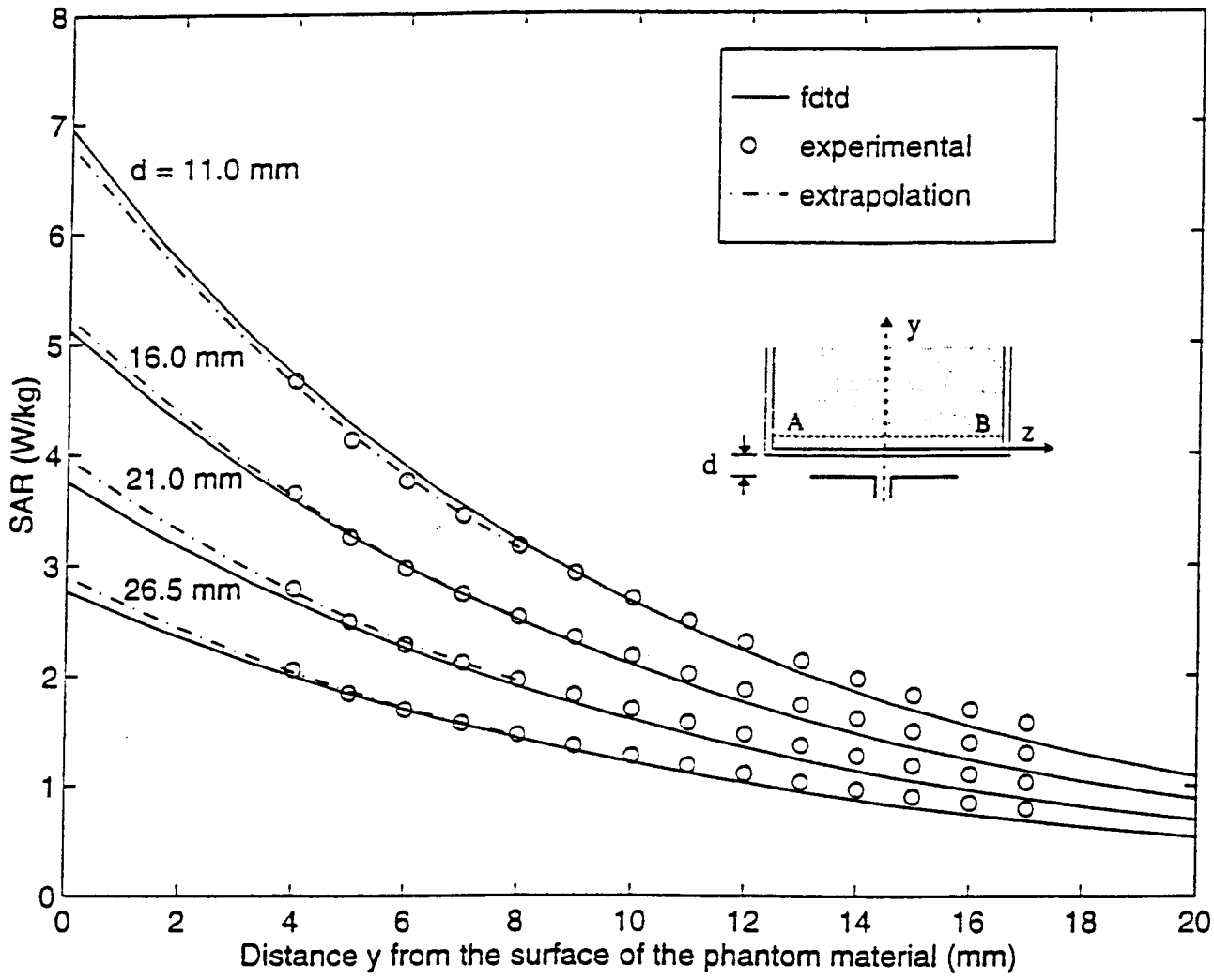

Fig. 5a. Comparison of the calculated and measured SAR variations for a box phantom of dimensions 30 × 15 × 50 cm; 840 MHz; λ/2 dipole antenna; 0.5 W radiated power. Calibration factor for the Narda Model 8021 probe at 840 MHz = 0.49 (mW/kg)/μV. Measured for the phantom material $\varepsilon_r = 41.1$, $\sigma = 1.06$ S/m.

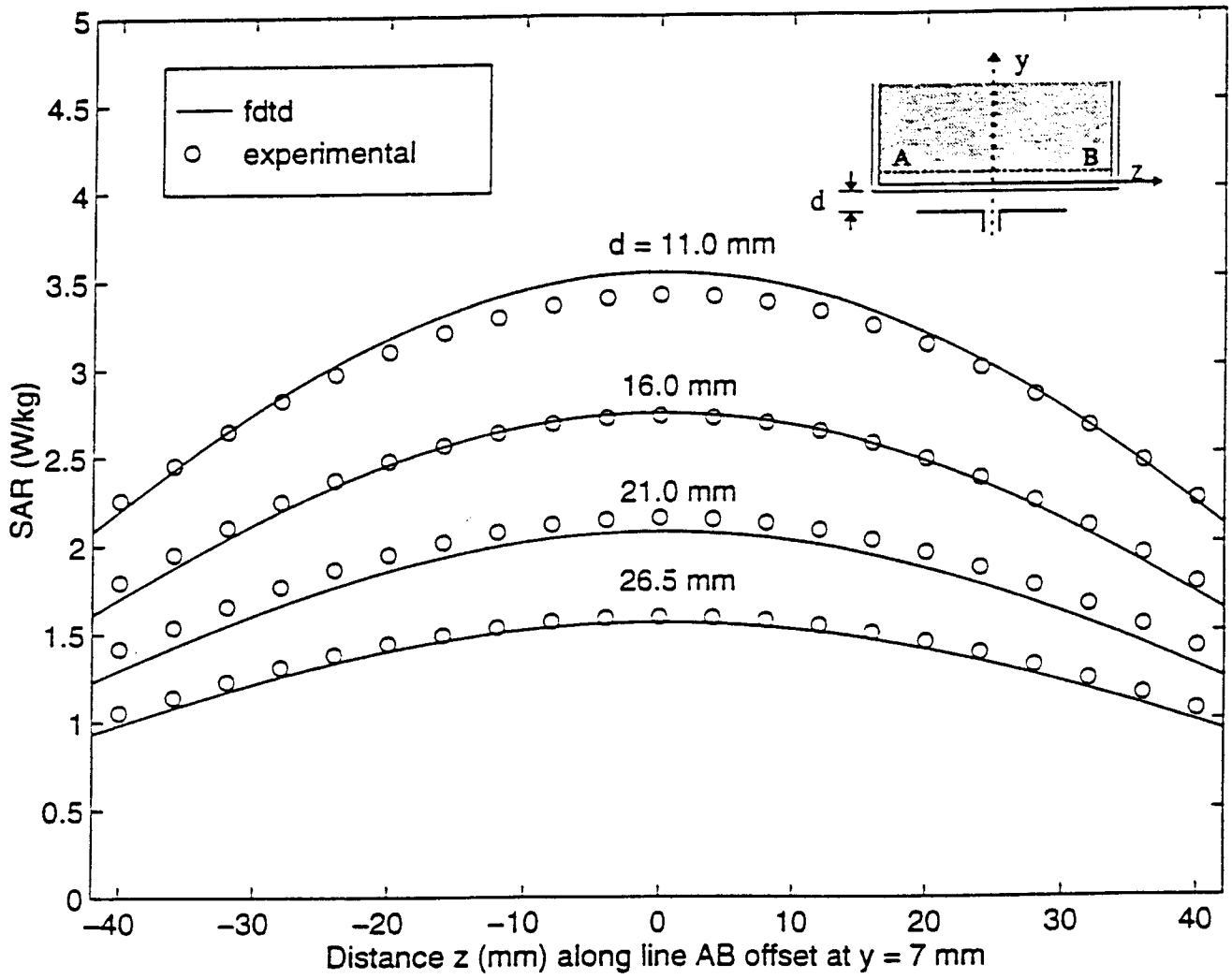

Fig. 5b. Comparison of the calculated and measured SAR variations for a box phantom of dimensions $30 \times 15 \times 50$ cm for a line AB parallel to the z axis at a distance y = 7 mm from the surface of the phantom material; 840 MHz; $\lambda/2$ dipole antenna; 0.5 W radiated power. Calibration factor for the Narda Model 8021 probe at 840 MHz = 0.49 (mW/kg)/μV. Measured for the phantom material $\varepsilon_r = 41.1$, $\sigma = 1.06$ S/m.

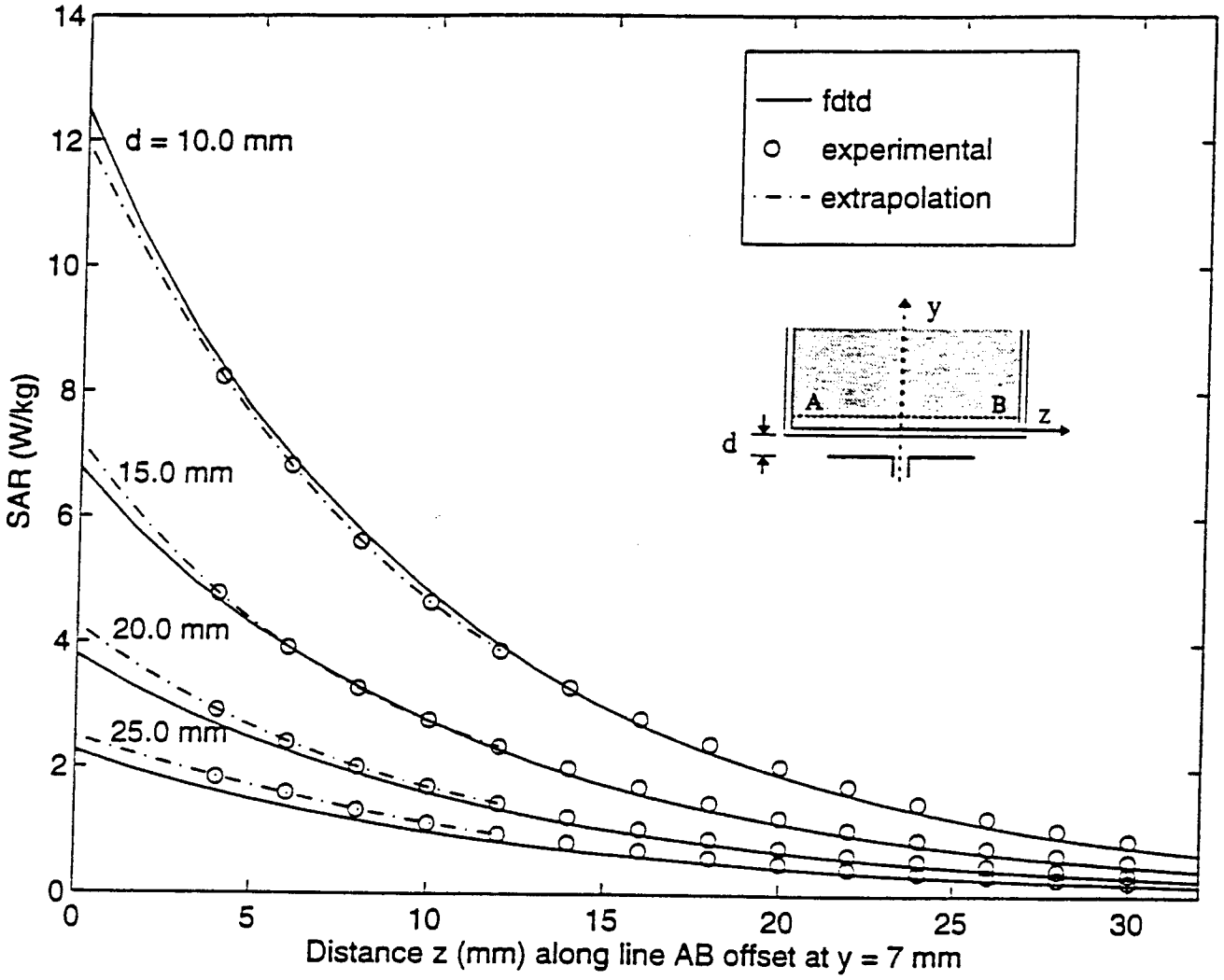

Fig. 6a. Comparison of the calculated and measured SAR variations for a box phantom of dimensions 30 × 15 × 50 cm; 1900 MHz; λ/2 dipole antenna; 0.5 W radiated power. Calibration factor for the Narda Model 8021 probe at 1900 MHz = 0.84 (mW/kg)/μV. Measured for the phantom material $\varepsilon_r = 45.5$, $\sigma = 1.31$ S/m.

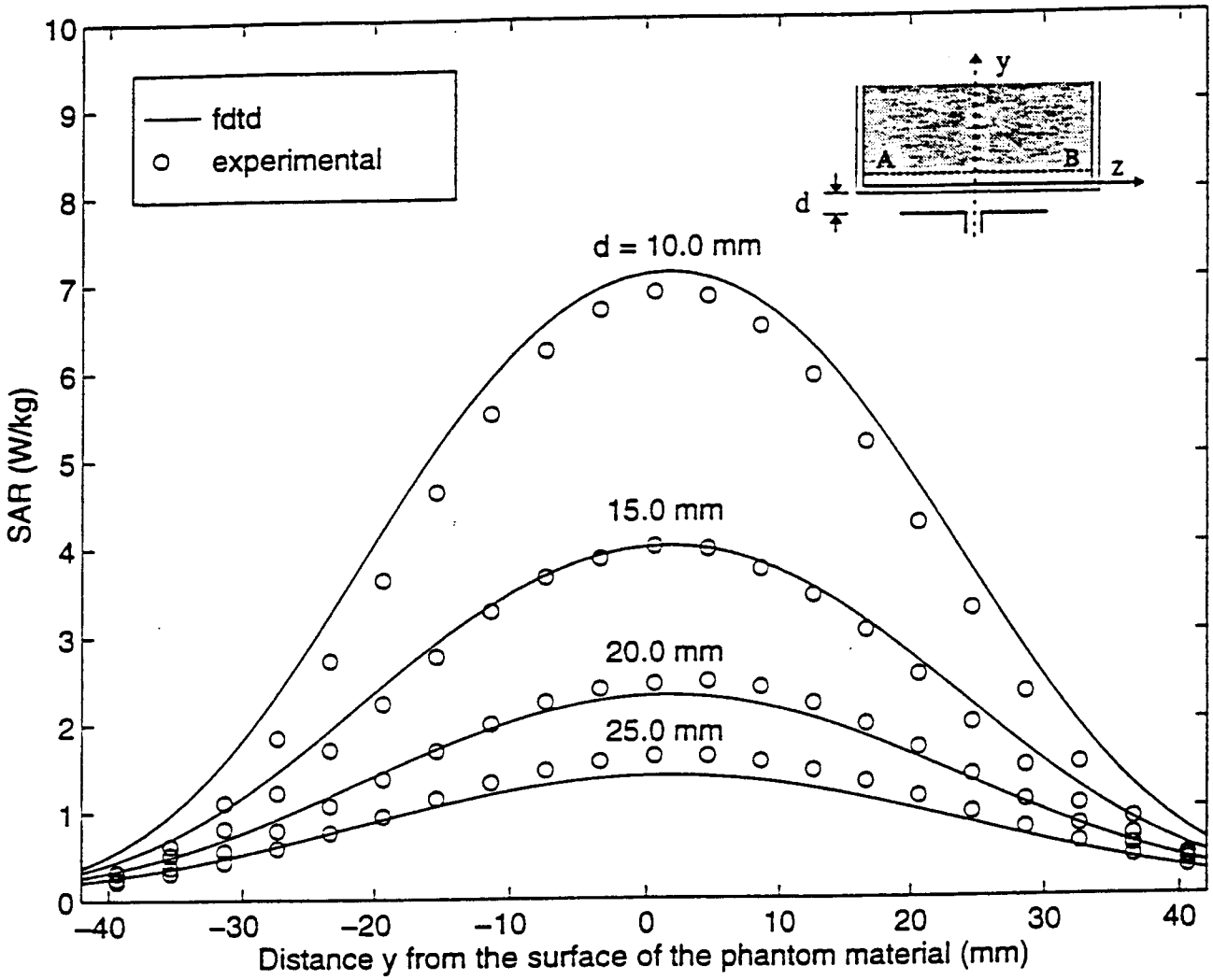

Fig. 6b. Comparison of the calculated and measured SAR variations for a box phantom of dimensions $30 \times 15 \times 50$ cm for a line AB parallel to the z axis at a distance y = 7 mm from the surface of the phantom material; 1900 MHz; $\lambda/2$ dipole antenna; 0.5 W radiated power. Calibration factor for the Narda Model 8021 probe at 1900 MHz = 0.84 (mW/kg)/μV. Measured for the phantom material $\varepsilon_r = 45.5$, $\sigma = 1.31$ S/m.

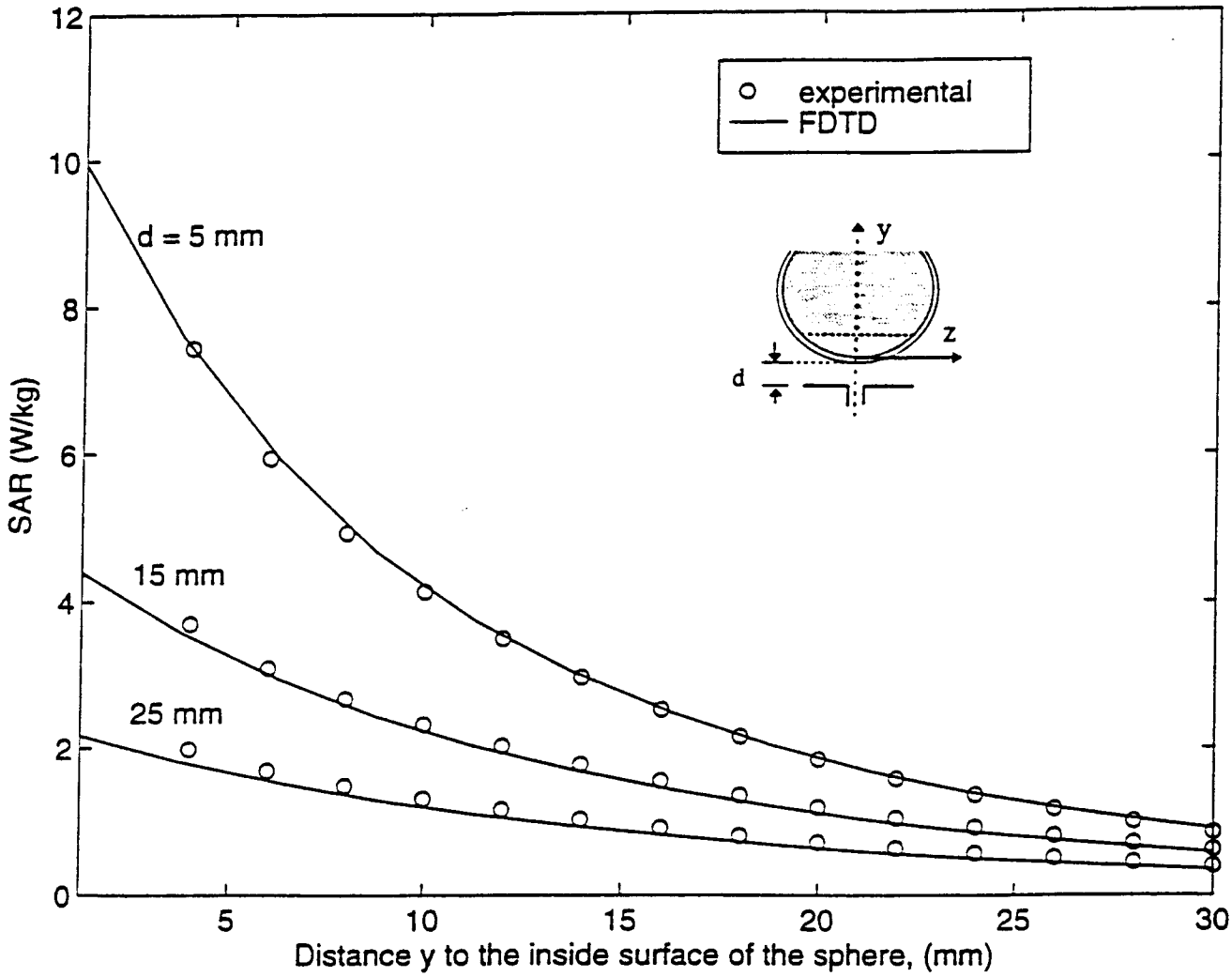

Fig. 7a. Comparison of measured and FDTD-calculated SAR variations at 840 MHz for a glass sphere model of outer diameter 22.3 cm and thickness 5 mm. SARs normalized to a radiated power of 0.5 W. Calibration factor = 0.49 (mW/kg)/μV. Measured for the phantom material $\varepsilon_r = 41.1$, $\sigma = 1.06$ S/m.

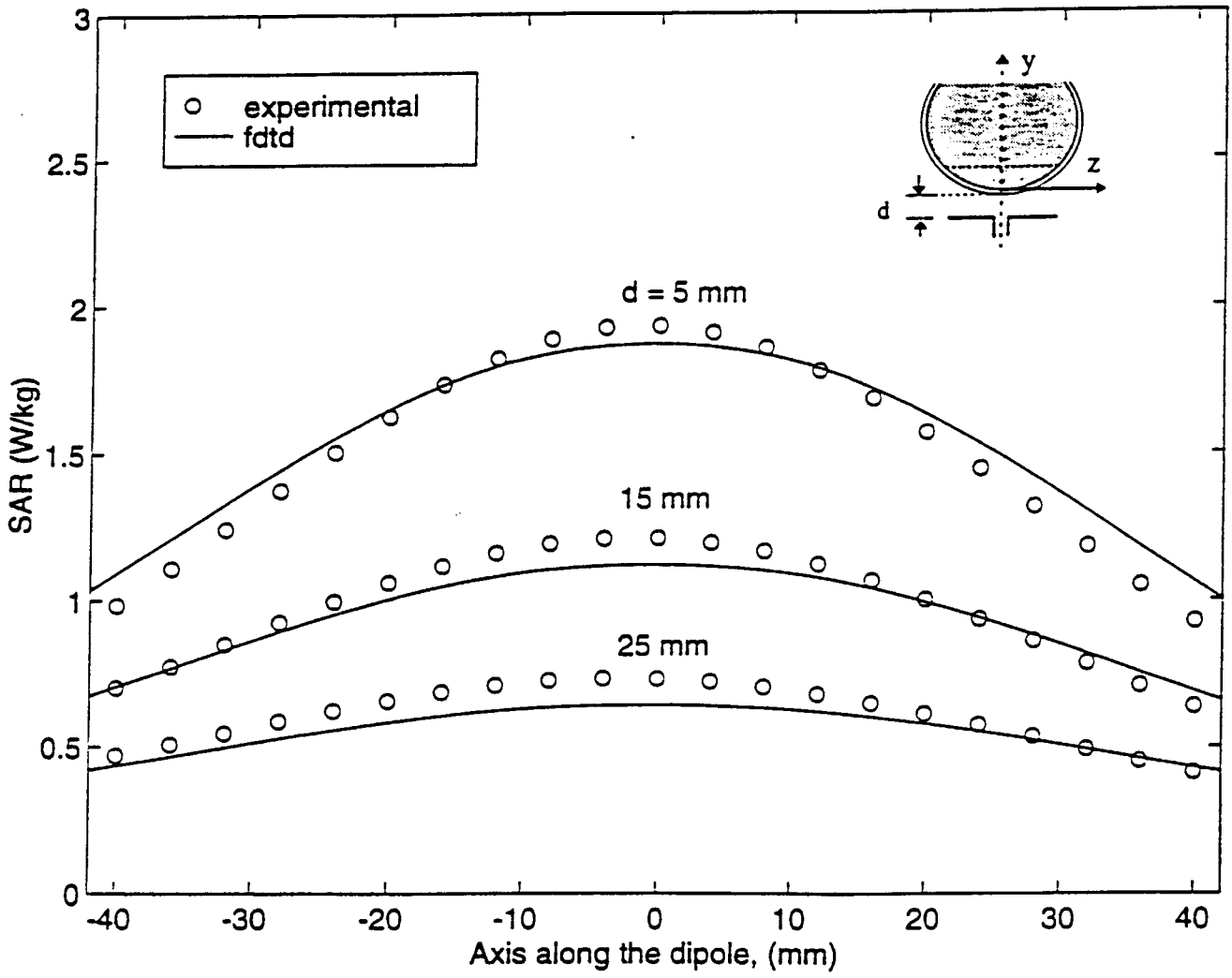

Fig. 7b. Comparison of calculated and measured SAR variations at 840 MHz for a plane at a distance of 20 mm from the lowest point on the inside of the sphere. SARs normalized to a radiated power of 0.5 W. Calibration factor = 0.49 (mW/kg)/μV. Measured for the phantom material $\varepsilon_r = 41.1$, $\sigma = 1.06$ S/m.

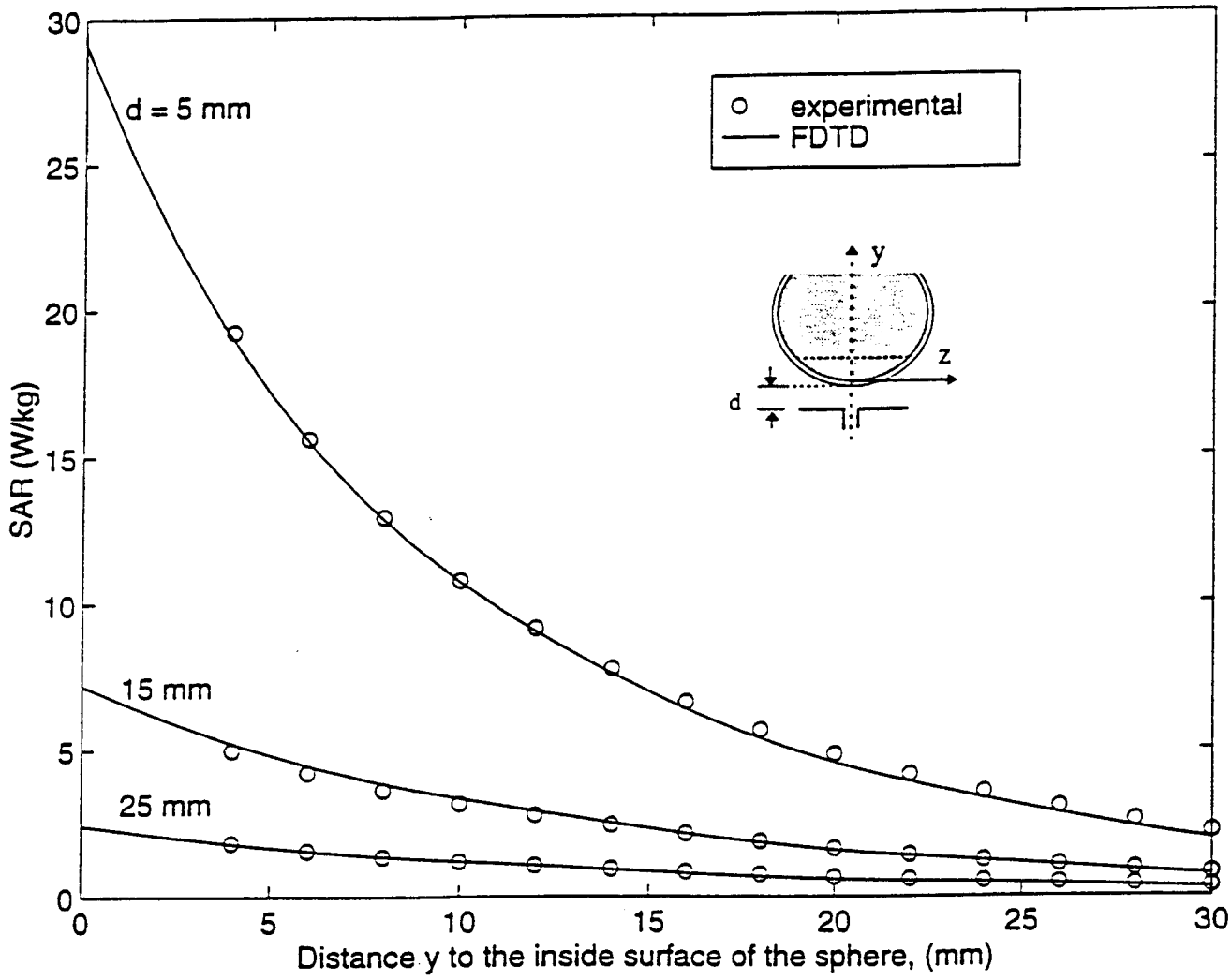

Fig. 8a. Comparison of measured and FDTD-calculated SAR variations at 1900 MHz for a glass sphere model of outer diameter 22.3 cm and thickness 5 mm. SARs normalized to a radiated power of 0.5 W. Calibration factor = 0.84 (mW/kg)/μV. Measured for the phantom material $\varepsilon_r = 45.5$, $\sigma = 1.31$ S/m.

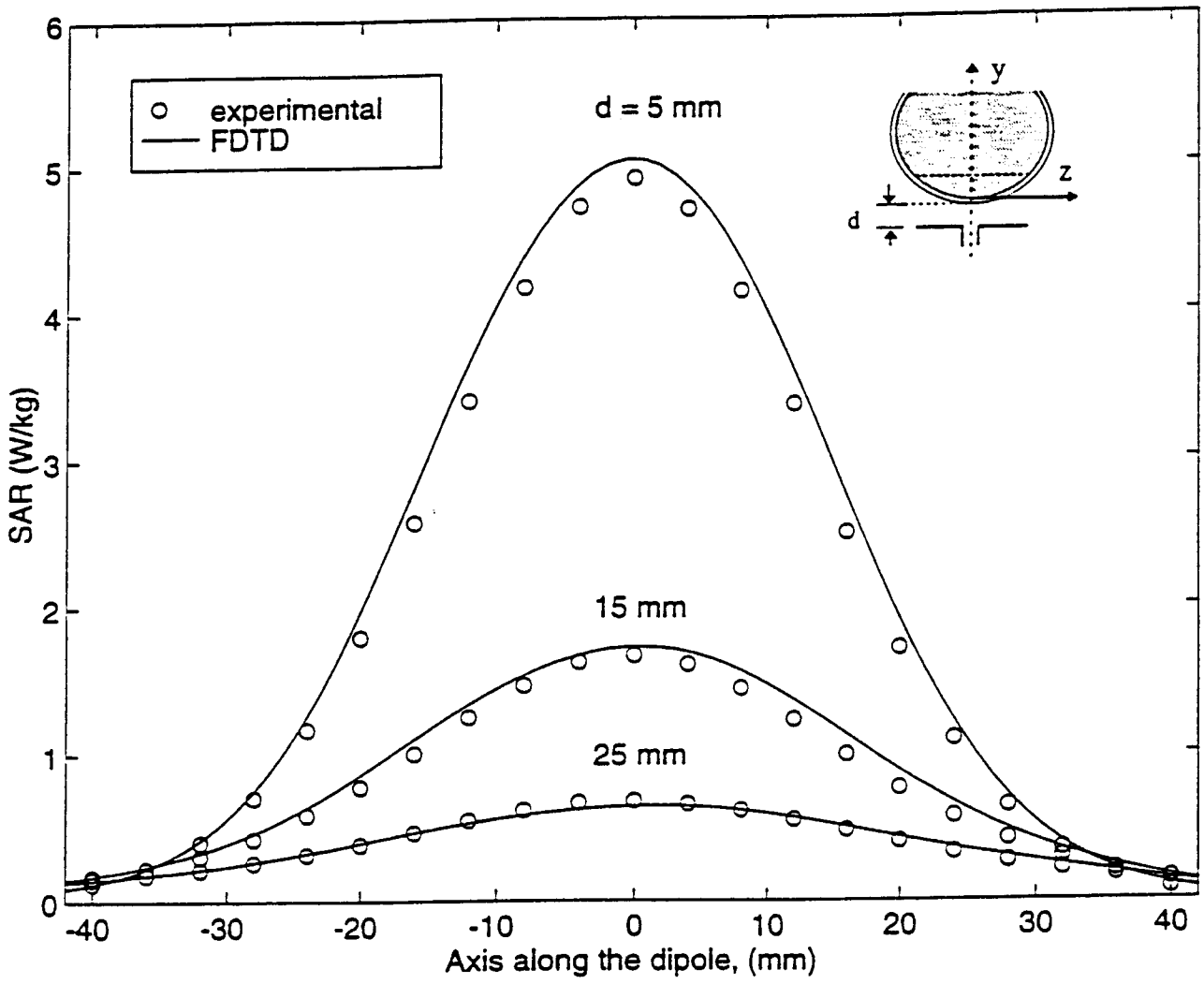

Fig. 8b. Comparison of calculated and measured SAR variations at 1900 MHz for a plane at a distance of 20 mm from the lowest point on the inside of the sphere. SARs normalized to a radiated power of 0.5 W. Calibration factor = 0.84 (mW/kg)/μV. Measured for the phantom material $\varepsilon_r = 45.5$, $\sigma = 1.31$ S/m.